Journal of Materials Chemistry A

Highly Uniform Nitride-rich Artificial Solid Electrolyte Interphase Enabled by Nano-Silicon Nitride for Superior Performance in Advanced Sodium Metal Batteries

Journal:	*Journal of Materials Chemistry A*
Manuscript ID	TA-ART-08-2024-005595.R1
Article Type:	Paper
Date Submitted by the Author:	24-Sep-2024
Complete List of Authors:	Damircheli, Roya; The Catholic University of America, Mechanical Engineering Hoang, Binh; The Catholic University of America, Mechanical Engineering Castagna Ferrari, Victoria; University of Maryland at College Park, Materials Science and Engineering; University of Maryland at College Park Institute for Research in Electronics and Applied Physics, Lin, Chuan-Fu; The Catholic University of America,

Highly Uniform Nitride-rich Artificial Solid Electrolyte Interphase Enabled by Nano-Silicon Nitride for Superior Performance in Advanced Sodium Metal Batteries

Roya Damircheli[1], Binh Hoang[1], Victoria Castagna Ferrari[2], Chuan-Fu Lin[1]*

[1]Department of Mechanical Engineering, Catholic University of America, Washington, DC, 20064, USA

[2] Department of Material Science & Engineering, University of Maryland, College Park, MD, 20742, USA

*Corresponding Author email: linc@cua.edu

Abstract

Sodium-metal batteries, notable for their high energy density and cost-effectiveness, face significant challenges such as dendritic sodium formation and unstable solid-electrolyte interphase (SEI), which hinder their operational safety and efficiency. Navigating through these challenges inherent in sodium-metal batteries, this research innovates by leveraging silicon nitride (Si_3N_4) to forge a robust sodium nitride (Na_3N)-rich artificial SEI layer. The Na_3N-rich SEI layer offers advantages such as improved mechanical stability and enhanced ionic conductivity, contributing to the overall performance of the battery. Through a cost-effective and straightforward methodology, the study showcases that optimized concentrations of 3wt % micro-Si_3N_4 and 1 wt % nano-Si_3N_4 enhanced cycling stability and diminished overpotentials. Although the micro-Si_3N_4 extends the sodium-metal symmetric cells' life to over 700 hours at 0.25 $mAcm^{-2}$ in carbonate-based organic electrolytes, the nano- Si_3N_4 variant excels, pushing the boundary to over 1000 hours, primarily due to its superior ability to form a highly uniform and dense SEI layer. These critical advancements, inhibiting dendrite growth and minimizing unnecessary SEI formation, signal a leap forward in developing safer, more resilient sodium metal battery technologies.

Keywords: Sodium Metal Anode, Anode Protection, Artificial SEI, Na_3N-rich Layer, Sodium Metal Batteries

1. Introduction

Sodium metal anodes are at the forefront of the evolution of sodium batteries, due to their promising and remarkable theoretical specific capacity of 1166 mAh/g and exhibit a low anode potential of -2.714 V compared to the standard hydrogen electrode.[1,2] However, this promise is overshadowed by the challenges that arise from their inherent reactivity and unstable nature during battery cycling.[3,4] A major challenge is the fragile and intractable dendrite growth during repeated electrochemical sodiation/desodiation processes as illustrated in Figure 1(a), leading to the formation of an unstable solid electrolyte interphase (SEI) due to interactions between metallic Na and liquid electrolyte. The sequential sodiation processes cause Na ions to accumulate beneath the SEI film on current collectors, resulting in significant volume expansions and leading to fractures in the SEI, thus paving the way for dendrites to grow through these fractures.[3,5] Also, this fluctuation triggers uneven ion movements, escalating into low Coulombic efficiency and inevitable dendrite progression, subsequently increasing impedance and decreasing overall energy efficiency.[6,7] If these dendrites continue to extend and propagate through the separator, they can cause internal short circuits within the cell, jeopardizing the safety and reliability of the battery. To overcome these obstacles and harness the full potential of Na metal anodes for high-energy and affordable sodium-ion batteries, it is crucial to innovate strategies for stabilizing the Na anode/electrolyte interface and suppressing the growth of Na dendrites.[8,9] This encompasses optimizing electrolyte mixtures, enhancing the sodium metal surface with either inorganic or organic thin coatings, and crafting sophisticated 3D current collectors.[10–12] Numerous studies and approaches have emerged, focusing on developing robust protective layers and stable artificial SEIs on sodium metal surfaces.[13–16]

In our previous study of stabilization of Na metal surfaces with a SnF_2 coating, we showed a significant extension of Na metal cycle life on a symmetric coin cell, with over 700 hours of operation, compared to approximately 200 hours with untreated Na anodes. [17] The fluorinated-SEI has been found to be crucial in suppressing dendrite formation, presenting a promising pathway to navigate and resolve pivotal challenges inherent in the deployment of sodium metal batteries. This stable layer also played a key role in preventing degradation and corrosion of the Na anode during cycling, suppressing electrolyte decomposition, and promoting uniform Na plating and stripping processes. The findings suggested the potential of SnF_2 as a viable alternative additive, contributing to the advancement of high-capacity and enduring energy storage systems by establishing NaF protection SEI layers.

Similar to the function of a NaF-rich SEI, incorporating a Na_3N-rich layer follows a similar principle. This strategy aims to aid in stabilizing sodium metal by facilitating an SEI which is rich in Na_3N compounds. The Na_3N compound within the SEI increases the variety of N^{3-} species present, leading to improved flow of Na^+ ions and faster diffusion through the SEI. This enhancement in ionic conductivity further reduces unwanted side reactions between the active metallic sodium and the electrolyte. [18]

Metal nitrates such as $LiNO_3$, $NaNO_3$, and KNO_3 exhibit a unique advantage in stabilizing sodium metal. These compounds, when dissolved in electrolytes, play a crucial role in forming a robust SEI. This SEI formation occurs through a reductive reaction with metallic Na, effectively alleviating side reactions with the organic electrolyte and suppressing dendrite growth. The significance of these SEI stabilizers lies in their ability to create an interphase structure rich in $N_xO_y^-$ and N^{3-} species within the SEI that leads to an enhancement in ionic conductivity, promoting smoother Na^+ diffusion through the SEI. Among these stabilizers, the metal nitrates stand out due to their capacity to foster N^{3-} rich species, contributing significantly to stabilizing sodium metal. In essence, the use of metal nitrates as SEI stabilizers proves advantageous in improving the interphase structure, enhancing ionic conductivity, and aiding in the overall stabilization of sodium metal by facilitating N^{3-} rich species within the SEI. [19,20]

The solid electrolyte interphase (SEI) is a critical layer that forms at the interface between the solid electrode and the liquid electrolyte in battery systems, facilitating the conduction of Na^+ ions. Broadly defined, the SEI refers to the interphase/interface layer that stabilizes the interaction between the electrode and electrolyte. More specifically, it can denote the decomposition layer that naturally forms due to electrochemical reactions during cycling. In our work, we utilize silicon nitride as an artificial SEI to effectively stabilize the sodium surface. This artificial layer facilitates the formation of a thin sodium nitride-rich layer, playing a crucial role in maintaining a stable interface. As commonly observed with bare sodium and lithium metal anodes, the electrolyte is continuously consumed during cycling, causing the natural SEI layer to grow thicker over time. However, the sodium interface is stabilized via the application of this artificial SEI layer by mitigating the undesired and uncontrolled electrolyte decomposition.

Si_3N_4 has been previously reported to act as a stabilizing agent in Li metal anodes upon electrochemical reaction and formation of Li_3N. The N^{3-} species promoted a higher diffusion of Li^+ on a similar mechanism when metal nitrides are used to stabilize the surface of Na metal. Therefore, it is expected that Si_3N_4 can also be used as coating layers in Na metal anodes for subsequent formation of Na_3N-rich SEI.[21,22] In this present study, not only we are the first to delineate this method, developing nitride-rich ASEI through applying thin layers of micro and nano-size Si_3N_4, as an innovative strategy for stabilizing Na metal anode, extending cycle life under high current conditions while inhibiting the development of dendrites, but also we investigate the protective effect of Na metal due to the surface distribution of various Si_3N_4 particle sizes, which is found to be important.

2. Experimental section

Materials and preparation

High-purity sodium metal cubes (99.9% purity), micro-sized powder (< 1μm), and nano-sized powder (< 50 nm and spherical) silicon nitride (Si_3N_4), dimethyl carbonate (DMC), ethylene carbonate (EC), and sodium hexafluorophosphate ($NaPF_6$), were purchased from Sigma-Aldrich Corporation. The electrolyte, 1 M $NaPF_6$ in a 1:1 EC:DMC solvent mixture, was prepared. Solutions with three different weight percentages (1, 3, and 5 wt %) of micro and nano Si_3N_4 in DMC were prepared and stirred for 24 hours prior to drop casting on the Na foils.

Inside an argon glove box to maintain a controlled atmosphere, all procedures were performed. The sodium metal cubes were cut carefully along the edges using a blade to reveal a glossy surface. Following that, the samples were pressed, rolled to attain a flat surface, and then cut into small discs using a 0.5-inch punch. Solutions containing various weight percentages of Si_3N_4 were drop-cast onto the sodium surface, each sample receiving a volume of 70 μL. After 48 hours of drying at room temperature, the treated sodium surfaces were rinsed with DMC to eliminate any unreacted residues and then dried for an additional 24 hours. Specific details of the fabrication methodology are described in supporting information S1.

Material characterization

Using the Hitachi SU-70 FEG, scanning electron microscopy (SEM) and energy dispersive spectroscopy (EDS) were performed to examine the surface morphology of untreated and treated sodium before and after cycling. To analyze the surface chemistry and elemental composition, we employed the Kratos Axis Ultra DLD XPS system, which featured an aluminum monochromated source, for X-ray photoelectron spectroscopy (XPS). Charge correction for the XPS spectrum was achieved utilizing the C 1s peak at 284.5 eV.

Electrochemical Characterization

Inside the argon glove box, symmetric cells were constructed utilizing CR-2032 coin-type cells. These cells incorporated both untreated sodium and sodium subjected to protection. To seal the cells, we applied 80 μL of 1 M $NaPF_6$ in a 1:1 EC:DMC electrolyte, along with two layers of Celgard 2400 separators. We then conducted plating/stripping performance assessments and impedance measurements for the symmetric cells using the Neware battery testing system (BTS8.0) and Gamry Electrochemical Impedance Spectroscopy (EIS), respectively.

3. Results and discussion

3.1 Formation of micro-Si_3N_4 and nano-Si_3N_4 artificial solid-electrolyte interphases

In Figure 1(a), pristine sodium is depicted, elucidating the inherent challenges it poses, notably during the sodiation/desodiation cycling process. These complications primarily arise due to the formation and growth of unpredictable dendrites amidst the cycling of sodium metal, attributed to recurring electrochemical plating and stripping processes. This scenario invariably leads to the creation of an unstable and uncontrollable SEI, a consequence of the immediate reaction between metallic Na and the liquid electrolyte[23]. The depiction demonstrates the fragile and non-uniform SEI layer formation that results in causing irregular ion movements leading to lower Coulombic efficiency and inevitable dendritic growth[24]. The continuous growth of the SEI layer impedes ion transport, resulting in increased polarization and decreased energy efficiency. During sodiation, a volumetric expansion occurs as Na ions tend to deposit on the Na anode or current collectors beneath the SEI film, leading to the fragmentation of the already fragile SEI. During repeated sodiation/desodiation, dendrites persist in their growth, propagating through the separator, culminating in a short circuit of the cell[25]. Conversely, Figure 1(b) elucidates the role of an artificial

Si_3N_4 SEI layer in safeguarding the sodium surface. This illustration is pivotal in demonstrating how the introduction of Si_3N_4 acts as a protective barrier against dendrite formation, thereby stabilizing the reactive sodium surface throughout repetitive stripping/plating processes.

This synthesized SEI layer served as a protective layer for the sodium surface, suppressing dendrite formation, and securing the highly reactive sodium anode throughout numerous stripping/plating cycles, highlighting the enhanced stability of the sodium surface post-sodiation and desodiation. The integration of Si_3N_4 is expected to facilitate the formation of a preferable artificial SEI layer that significantly mitigates the risks associated with the instability of pristine sodium, offering a robust and reliable approach to stabilizing sodium metal. This methodology underscores the potential advancements in sodium stabilization and reveals the prospective benefits in the broader spectrum of sodium metal battery technologies.

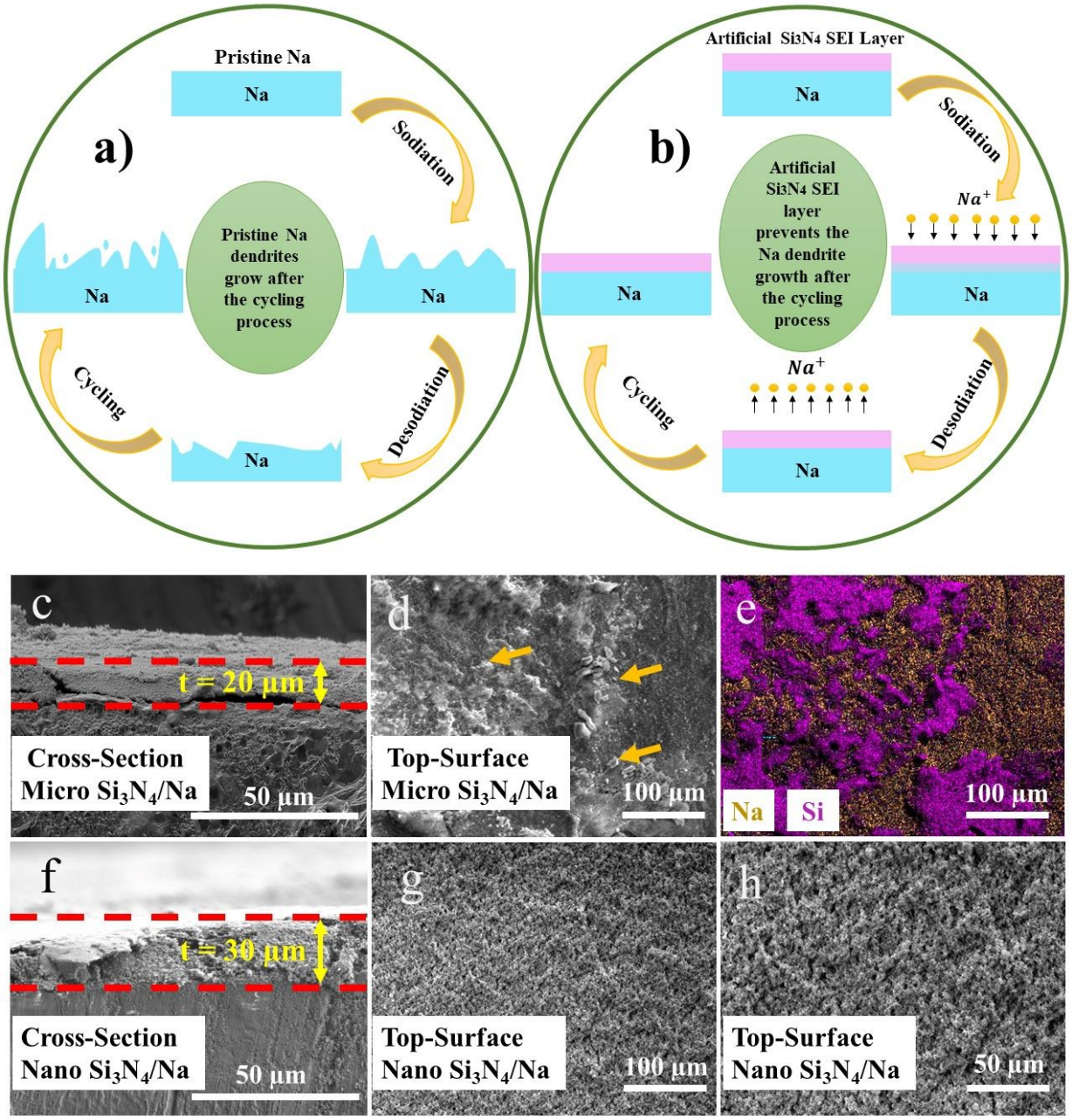

Figure 1: Schematic illustration detailing a) the growth of Na dendrites on pristine Na metal, b) the uniform Na stripping /deposition on the established artificial Si_3N_4 SEI layer on the Na metal, c) the cross-section of micro-sized 3 wt % Si_3N_4/Na as-prepared, d) the high-resolution top-view SEM images of micro-sized 3 wt % Si_3N_4/Na as-prepared, e) the corresponding EDS of the area in d), f) the cross-section of nano-sized 3 w t% Si_3N_4/Na as-prepared, g), h) the high-resolution top-view SEM images of nano-sized 3 wt % Si_3N_4/Na as-prepared.

The as-prepared cross-section and top-surface morphology of the 3 wt % micro-sized Si_3N_4 treated sodium metal were first investigated using scanning electron microscopy (SEM), with the findings illustrated in Figure 1(c,d). 3 wt% was chosen as the starting point due to the limitations in the

dispersion of silicon nitride in dimethyl carbonate (DMC). Detailed examination of the cross-section reveals the formation of a 20-micron layer on the sample's surface. A meticulous examination of Figure 1(d) unveils insights into the surface morphology, displaying a lack of smooth and uniform distribution of micro-Si_3N_4 across the sample. Though a comprehensive coverage of micro-Si_3N_4 is observed, there is a notable variation in the thickness of the coverage across different regions, which resembles isolated islands and indicates non-uniform aggregation of micro-Si_3N_4 at certain locations as mentioned with arrows in Figure 1(d). Energy dispersive spectrum (EDS) mapping, as represented in Figure 1(e), was conducted to acquire elemental information on the analogous region explored in 1(d). Figure 1(e) shows an uneven distribution of micro-Si_3N_4 across the surface, with exposed regions of sodium metal, and creates surface heterogeneity. Surprisingly, despite the non-uniform coverage of micro-Si_3N_4 on the Na surface, the notable performance during long-term cycling was observed and will be discussed in depth in section 3.3.

In addressing the issue of non-uniform coverage due to incomplete dispersion of micro-sized ceramic particles of Si_3N_4, our approach extended to the utilization of nano-sized Si_3N_4 particles to hope to overcome the persistent challenge posed by the limited coverage of the micro-Si_3N_4. Therefore, our ongoing research pivots towards exploring the impact and efficacy of nano-sized powder of Si_3N_4 (< 50 nm) on the coverage of the Na surface and how the surface coverage conditions affect the long-term cycling performance of Na metal anode.

As depicted in Figure 1(f), a denser and more uniformly structured layer of nano-Si_3N_4 has formed, measuring 30 μm in thickness. Notably, this improved formation of the layer demonstrates not only increased thickness but also enhanced adhesion to the sodium surface, resulting in superior contact between the layer and the sodium surface. Figure 1(g-h) illustrates the surface morphologies of the nano-Si_3N_4 treated Na metal, in which they show improved uniformity of the layer, affirming the superior coverage of nano-Si_3N_4 compared to micro-Si_3N_4 in Figure 1(d). A magnified view of the surface morphology of the nano-Si_3N_4 Figure 1(h) showed no sign of agglomeration of particles from the SEI. While Na metal should have a smooth surface, as depicted in uncoated regions in Figure 1(e), the nano-Si_3N_4 coated Na metal presented a regular surface roughness, which evidences a uniform distribution of particles. The transition from adopting micro-Si_3N_4 particles to nano-Si_3N_4 particles appears to have significantly improved the coverage of the Si_3N_4-based artificial SEI layer to the Na surface. The effects of the particle sizes and the coverage of Si_3N_4 to the stabilization of Na metal anode via electrochemical characterizations are investigated and reported in the following sections.

3.2 XPS Quantification of artificial SEI

For evaluation of the surface chemistry after coating Na metal anodes with Si_3N_4, X-ray Photoelectron Spectroscopy (XPS) was employed to examine the elemental composition, as shown in Figure 2. Two distinct samples underwent XPS analysis: (1) as-prepared 3 wt % micro-Si_3N_4 coated Na sample, as shown in Figure 2(a) for the survey spectrum, and (2) 3 wt % micro-Si_3N_4 coated Na sample subjected to 400 hours of cycling, as shown in Figure 2(b) for the survey spectrum. In Figure 2(a), Si 2p and N 1s peaks are prominently shown, which reveals the coating of Si_3N_4; at the same time, the suppressed Na 1s peak is shown, which indicates the buried Na

surface underneath a reasonable coverage of the Si_3N_4 layer although the uniformity is limited, as it was confirmed by EDS analysis in Figure 1(c).

In Figure 2(b), after 400 hours of cycling, the Si 2p and N 1s peaks are still noticeable but suppressed, indicating the formation of natural solid-electrolyte-interphase (SEI) from electrolyte decomposition. As the high-intensity peaks shown in Figure 2(b), the natural SEI is comprised of Na, C, F, and O, which are the major elements from the $NaPF_6$-based carbonate liquid electrolyte.

In Figure 2(c) and 2(d), the high-resolution XPS spectra of N 1s and Si 2p are shown, respectively, from the as-prepared 3 wt % micro-Si_3N_4 coated Na sample. For N 1s, two major N peaks are observed and assigned to $SiN_{1.33}$ (same as Si_3N_4) at 397.4 eV and SiN_x ($x \sim 0.44$) at 396.1 eV based on the calculation of the atomic ratios[26–28]. Furthermore, the identification of a small peak at 400.4 eV unfolds the compositional nuances of the treated sodium surface with the implications of the formation of a thin Na_3N interface[29]. This agrees with the proposed conversion reaction at the interface of Si_3N_4 with Na metal as below, where the silicon is reduced and loses nitrogen during sodiation process that forms Na_3N[29]:

$$Si_3N_4 + 12\,Na \rightarrow 3\,Si^{\circ} + 4\,Na_3N \qquad (1)$$

The surface chemistry and the reaction are supported by high-resolution Si 2p spectrum, shown in Figure 2(d). $SiN_{1.33}$ and SiN_x peaks are observed and labeled at 102.5 eV and 101.5 eV, respectively. Reduced Si metal peak, labeled at 99.3 eV, is observed, confirming the proposed interfacial reaction in (1).

The high-resolution XPS spectra of N 1s and Si 2p of 400-hours cycled sample are shown in Figure 2(e) and 2(f). After long cycles, the amount of $SiN_{1.33}$ reduces significantly, where low N content SiN_z ($z \sim 0.8$), with N 1s peak at 397.0 eV and Si 2p peak at 101.1 eV, dominates the remaining composition. The decrease in nitrogen content from $SiN_{1.33}$ (Fig 2(d)) to $SiN_{0.8}$ (Fig 2(f)), channeled towards the formation of larger amounts of Na_3N for after-cycled composition.

The formation of Na_3N, known for exhibiting high stability against Na metal anode with high ionic conductivity[30,31] , as desired artificial SEI, plays a key role in facilitating smooth and uniform movement of Na^+ ions, which is pivotal for suppressing dendrite formation, reducing electrolyte decomposition, and improving the overall efficiency. The presence of interfacial Na_3N throughout the whole long-cycling process ensures the long-term stability and performance of sodium-based batteries, which were confirmed from our electrochemical cycling measurements.

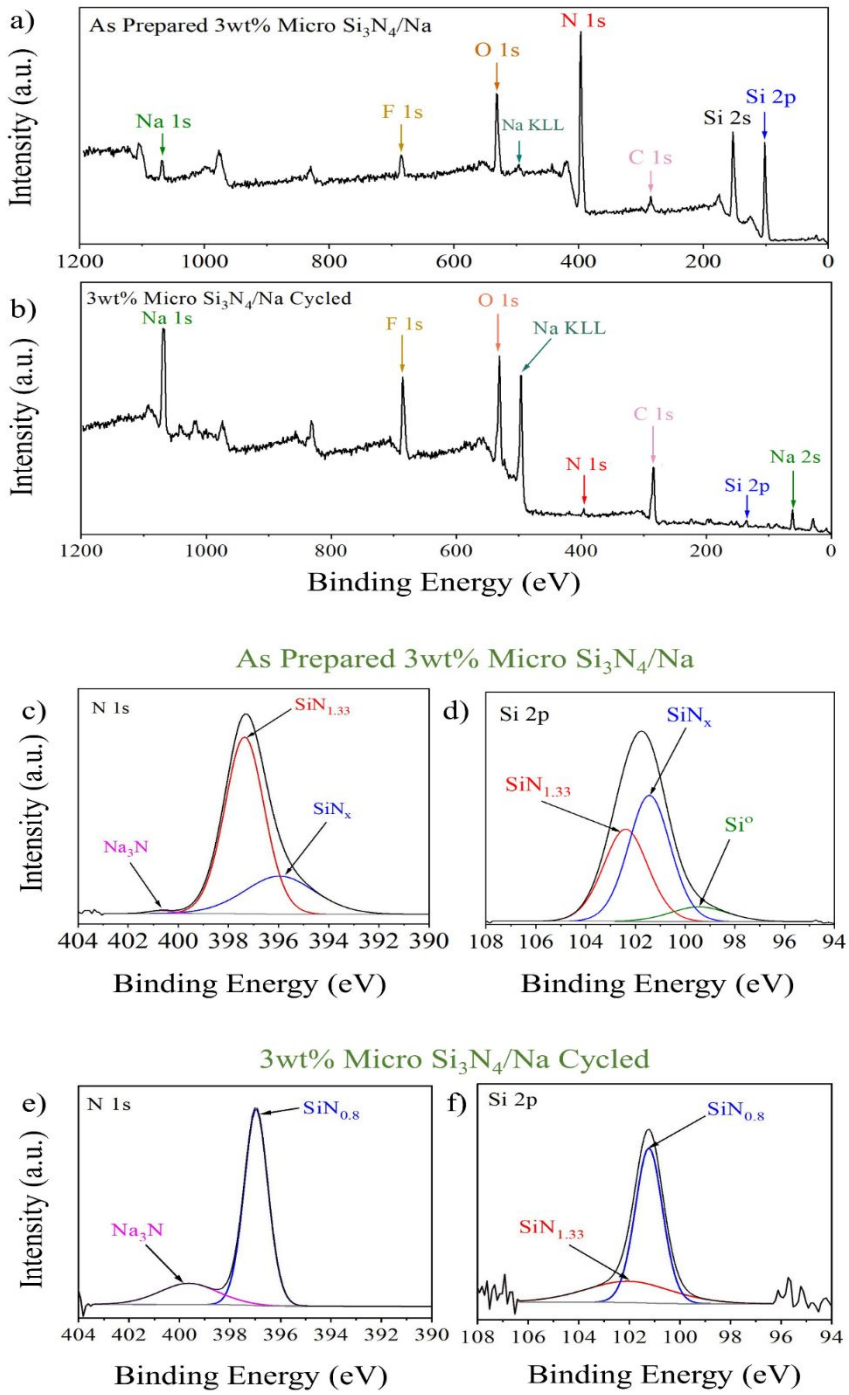

Figure 2. a) XPS survey spectra of as prepared 3 wt % micro-sized Si_3N_4/Na, b) 3 wt % micro-sized Si_3N_4/Na cycled, c,d) High-resolution XPS spectrum of N 1s and Si 2p of as-prepared 3 wt % micro-sized Si_3N_4/Na, e,f) 3 wt % micro-sized Si_3N_4 /Na cycled.

3.3 Electrochemical Performance and Characterizations

The cyclic deposition and stripping processes of symmetric cells utilizing 3 wt % micro-Si_3N_4 and nano-Si_3N_4 coated Na metal and bare Na metal are shown in Figure 3(a), performed under a constant current density of 0.25 mA cm^{-2} with each cycle pre-determined to last 30 minutes. The micro-Si_3N_4 coated Na metal manifests stable cycling performance, minimal overpotentials and voltage fluctuations, and upholding symmetric cyclability for up to 700 hours, which it indicates the effectiveness of the micro-Si_3N_4 artificial SEI layer to extend >3x the lifetime of Na metal anode. This is attributed to the formation of the desired interface, Na_3N, throughout the battery cycling, described in the following section. Despite the limited coverage and uniformity of the micro-Si_3N_4 on Na metal as indicated in Fig. 1(e), it still facilitated the formation of the preferable Na_3N interface, ensuring the extended cycle life of the Na metal, which is a feature absent in the bare Na cells. The utilization of nano-sized Si_3N_4 not only exhibited much improved surface coverage on Na metal, as shown in Fig. 1(h), the nano-Si_3N_4 treated Na anode exhibited a notably enhanced cycling performance, demonstrating extra high stability and remarkable cyclability that reached approximately 1000 hours - 5x higher than the bare Na sample. This prolonged cycling duration emphasizes the effectiveness of the uniform coverage of nano-Si_3N_4 protection layer in enhancing the overall cycling efficiency and longevity of sodium anode.

The pristine Na cells, conversely, revealed rapid increases in overpotentials around 5 V, leading to the ultimate cell failure, due to the formation of uncontrollable and unstable SEI at the bare sodium interface. The sharp contrast of the performance between bare-Na and Si_3N_4-treated Na highlights the critical role of Na_3N-rich SEI layer to the enabling of a stable and robust Na anode.

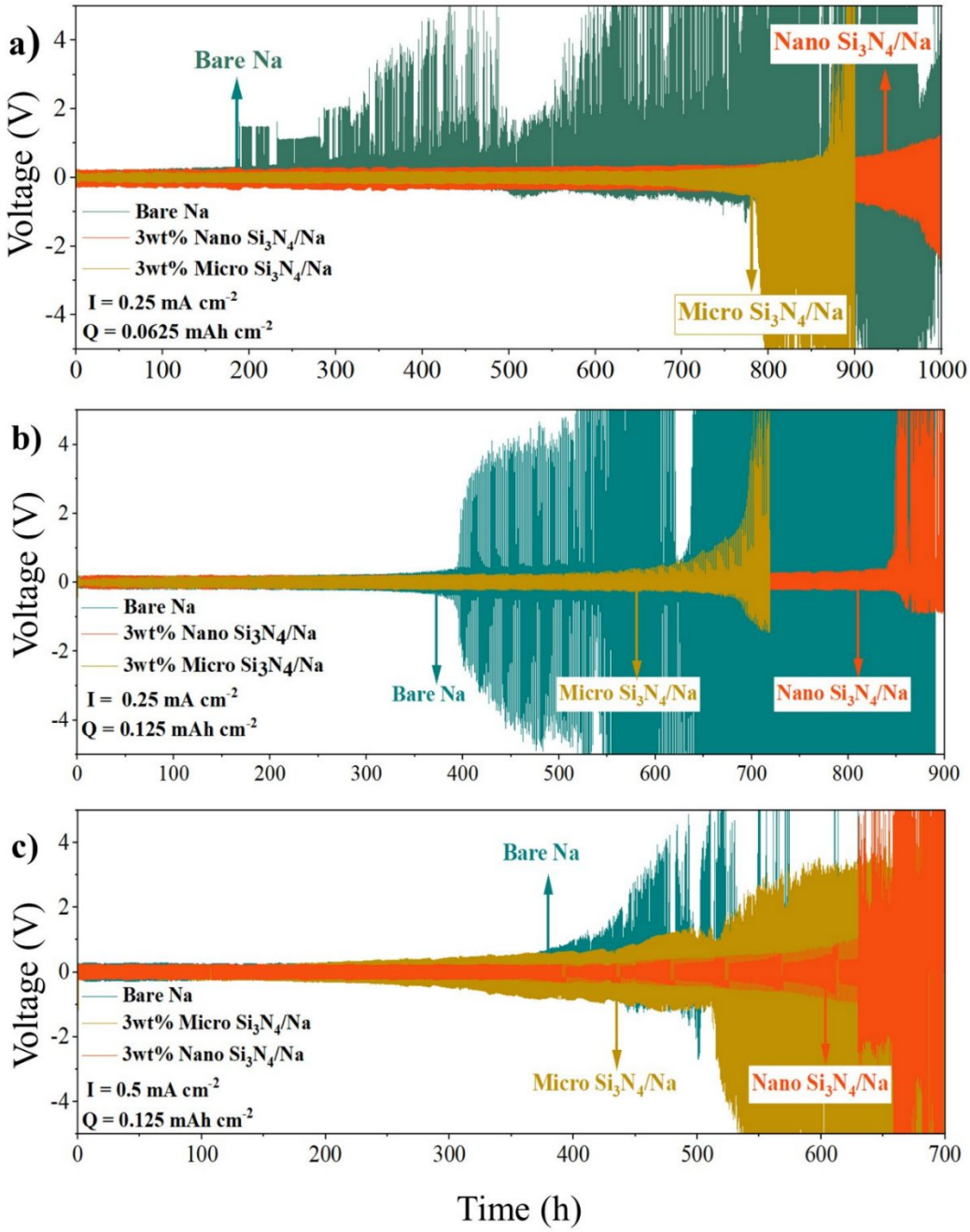

Figure 3. a) Cyclic deposition/stripping process of symmetric cells using 3 wt % micro and nano-sized Si_3N_4 coated Na metal and bare Na metal at a constant current density of 0.25 mA cm^{-2}. Each cycle is set to be 30 min. b) Each cycle is set to be one hour. C) Cyclic deposition/stripping process of symmetric cells using 3 wt % micro and nano-sized Si_3N_4 coated Na metal and bare Na metal at a constant current density of 0. 5 mA/cm^2 and each cycle is set to be 30 min.

The nanopowder's finer granularity facilitates a more efficient distribution within the solvent, ensuring a more consistent and homogeneous application across the metal surface. This uniform dispersion is crucial for achieving a coherent and evenly distributed coating layer. Moreover, the increased surface area inherent to nano-scale particles significantly strengthens their adherence to the metal substrate, a pivotal factor in the durability and effectiveness of the coating. This augmented adhesion not only contributes to a denser coating layer but also ensures a more stable and enduring performance. The integration of nano-Si_3N_4 thus represents a substantial advancement in the coating, offering significant improvements in both the application process and the longevity of the coating.

In Figure 3(b), the examination was conducted by doubling the time for each charge/discharge cycle to one hour, to assess the performance of the cells under deep charge/discharge conditions. When the cycling time was doubled, the pristine sodium cells began to fail by showing large voltage overpotentials after 400 hours; conversely, the micro-Si_3N_4 treated Na cells exhibited enduring stability, surviving beyond 670 hours; finally, the nano-Si_3N_4 treated Na cells has reached over 840 hours. This superior stability and cycle life evidenced the uniform and desired Na_3N-rich interface, facilitated by the nano-Si_3N_4, is highly effective to stabilize the Na anode surface from forming dendrites and to reduce the undesired natural SEI formation.

Furthermore, to evaluate the protection effect at an even higher current density, bare Na, micro-Si_3N_4 treated Na, and nano-Si_3N_4 treated Na were conducted with cyclic deposition/stripping processes of symmetric cells at an escalated constant current density of 0.5 mA/cm^2, which is shown in Figure 3(c). It was observed that when the current density was doubled, the bare Na metal showcased a decline in stability and the onset of voltage hysteresis occurred swiftly. Contrarily, the cell integrated with micro- and nano-Si_3N_4 maintained its stability for up to 500 and 630 hours, illuminating the remarkable enhancements afforded by the Si_3N_4 coating at higher current densities. This denotes the profound efficacy of Na_3N-rich SEI layer formation in augmenting the stability of Na metal anodes across varying operational parameters, fortifying its standing as a promising solution in the realm of sodium stabilization technologies.

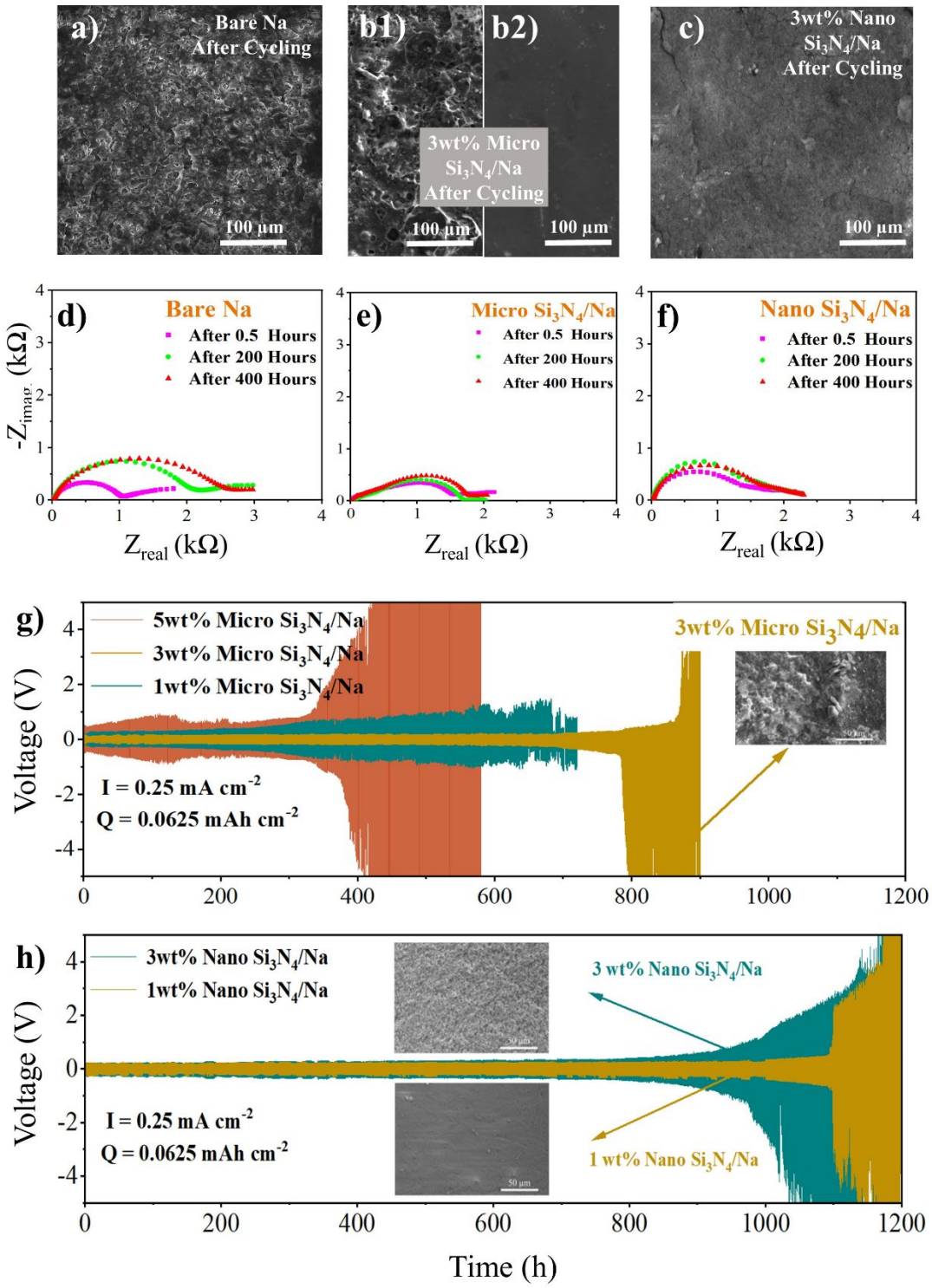

Figure 4. Top-view SEM images of a) bare sodium, b1, b2) 3 wt % micro Si_3N_4/Na and C) nano Si_3N_4 after 400 hours of long-term cycling. EIS spectra of symmetric cells using d) bare Na metal, e) micro size Si_3N_4 coated sodium, f) nano size Si_3N_4 coated sodium after 0.5, 200, and 400 h of cycling. Each cycle is set to be 30 min. g) Cyclic deposition/stripping process of symmetric cells using 1, 3, and 5wt% micro Si_3N_4/Na metal at a constant current density of 0.25 mA cm^{-2}. Each cycle is set to be 30 min. h) Cyclic deposition/stripping process of symmetric cells using 1, and 3wt% nano Si_3N_4/Na metal at a constant current density of 0.25 mA cm^{-2}. Each cycle is set to be 30 min

We further conducted postmortem examination utilizing SEM to elucidate the impacts of Si_3N_4 coating to the Na surface morphologies under long-term cycling Na, as shown in Figure 4(a-c). For the bare Na (Figure 4(a)), extensive cycling revealed the formation of pronounced three-dimensional structures, indicative of non-uniform Na deposition, leading to erratic dendrite formation and growth, exacerbating electrolyte decomposition and SEI formation. This, coupled with observable large amounts of dead and mossy Na due to significant electrolyte consumption, resulted in the drying up of the cells and substantial overpotentials after 400 hours of cycling. Figure 4(b_1, b_2) displays the top-view SEM images, illustrating the morphological alterations in micro-Si_3N_4 coated Na cells after 400 hours of cycling. A clear discrepancy was observed on the surface areas, with approximately 50% depicting agglomerated and uneven surfaces, as shown in Figure 4(b_1), and the remaining 50% illustrating smoother and more uniform surfaces, akin to Figure 4(b_2). The former, characterized by elevated, non-uniform islands, potentially points to areas of agglomerated parts on the surface of as-prepared samples, indicative of morphological inconsistencies, as shown in Figure 1(d). However, despite the uneven surface morphologies, the presence of the thin Na_3N-rich artificial SEI layer, suggested by XPS from Figure 2(c), effectively stabilizes the Na surface to largely enhance the cycle life of Na anode and cell kept its original state after 400 hours of cycling. As it is shown in Figure 4(c), a highly uniform surface was observed after 400 hours of cycling of the nano-Si_3N_4 coating, with no traces of any dendrite formation or three-dimensional structures. The sample kept its original state after cycling, which is confirming the uniform and even distribution of nano-size Si_3N_4 can progressively enhance the stable interphase after cycling.

The charge transfer impedance and interfacial stability for both bare Na, micro-Si_3N_4/Na and nano-Si_3N_4/Na cells underwent an evaluation using electrochemical impedance spectroscopy (EIS). Nyquist plots depicted notable distinctions in the charge transfer impedance over cycling durations of 0.5, 200, and 400 hours between bare Na, micro-Si_3N_4/Na and nano-Si_3N_4 samples, as shown in Figure 4(d-f). In Figure 4(d), the significant and continuous increase in charge transfer impedance, roughly a threefold rise over 400 hours, was observed in bare Na. This is due to the continuous formation of the undesirable and unmanageable natural SEI during cycling that led to the continuous increase of the impedance. Conversely, the micro-Si_3N_4/Na samples in Figure 4 (e) showcased highly stable interfacial impedance over the 400-hour cycling duration, indicating that the Si_3N_4 artificial SEI effectively boosted the stability of Na metal through suppressing the parasitic reaction that forms undesired natural SEI, which aligns with the findings in cycling performance. The nano-Si_3N_4/Na impedance profile in Figure 4(f) showed a very small charge-transfer resistance changes over 400 hours of cycling, revealing the better and more uniform layer for transferring the ions formed in comparison to the bare sodium. After hours of cycling, the interfacial impedance stayed highly stable. Interestingly, both the micro- and nano-Si_3N_4 coatings on Na metal led to similar ranges of charge-transfer resistance (1500 – 1800 Ω) after several hours of cycling. This impedance analysis confirms that, regardless of the particle size and/or uniformity of Si_3N_4 coating, the established artificial SEI layer successfully prevents side reactions with Na

for suppression of Na dendrite growth for extended periods of cycling. Given that the micro and nano coatings show similar impedance behavior, their chemical compositions are expected to be similar as well. Therefore, conducting XPS analysis only on the micro sample is sufficient, as it would provide results comparable to those of the nano sample.

Our exploration into the impact of varying weight percentages of micro- and nano-Si_3N_4 SEI layers on the stability of Na metal anodes was illustrated in Figure 4(g-h). Na samples treated with 1, 3, and 5 wt % of micro-Si_3N_4 and 1 and 3 wt % of nano-Si_3N_4 and their performances were analyzed. The cycling was conducted with the current density fixed at 0.25 $mAcm^{-2}$, with each cycle of half an hour. Discrepancies in performance were noted between the different concentrations. In Figure 4(g), the 1 wt % micro-Si_3N_4 seemed suboptimal, likely due to its inability to sufficiently cover the entire surface, leading to exposed areas and compromised protection. Conversely, the 5 wt % micro exhibited elevated overpotentials due to a consequence of the excessive concentration and resultant layer thickness that impedes ion mobility. The 3 wt % micro-Si_3N_4 showcased the optimal stability and the lowest overpotential over 750 hours.

For the case of the nano-Si_3N_4 protection layer, as shown in Figure 4(h), while the 3 wt % nano-Si_3N_4 demonstrated stable and superior cycling to last around 1000 hours, the 1 wt % nano-Si_3N_4 treated Na shows even better stability and efficiency of cycling to last 1100 hours. Both 3 wt % and 1 wt % nano-Si_3N_4 facilitate uniform surface coverage of the layer that gives rise to the superiority of the cycling performance, and due to the smoothness of the layer coverage, the 1 wt% nano-Si_3N_4 is sufficient to ensure the full coverage and formation of the preferable Na_3N-rich thin SEI layer – thus slightly reduces the overpotential and increases the cycle life.

Our findings suggest that the low concentration of nano-Si_3N_4 is most effective to stabilize Na metal anode surface due to the highly uniform coverage of the protective layer that led to the formation of a thin and homogenous Na_3N artificial SEI, and to minimize the unnecessary thick layer that often impede ion transport. Here, we report a novel development of a low-cost strategy to stabilize Na metal anode for 5x superior cycling performance. Future endeavors could be directed toward refining the optimization process, enhancing our understanding of the intricate interplay between layer thickness, ion mobility, and overall anode stability. [35–37]

4. Conclusion

This study represents a significant advancement in the realm of sodium-ion battery technology, particularly in the stabilization of sodium metal anodes. Initially, our approach with micro-sized silicon nitride (Si_3N_4) yielded a Na_3N-rich artificial solid electrolyte interphase (SEI) with a reduced and controlled charge-transfer resistance in comparison to a bare Na metal, a key factor in enhancing sodium anode stability. However, the microscale application encountered challenges in achieving uniform SEI coverage. This led to a pivotal shift towards employing nano-sized Si_3N_4, resulting in a marked improvement in the uniformity and integrity of the SEI layer. The use of nano Si_3N_4 not only addressed the coverage uniformity but also significantly enhanced the electrochemical performance, extending the operational life of the batteries to over 1000 hours, compared to the 700 hours achieved with micro-sized Si_3N_4. This notable increase, compared to

the micro-sized variant, underscores the effectiveness of nano Si_3N_4 in creating a more robust and efficient Na_3N-rich SEI layer. This research thus provides a crucial insight into the potential of nano-engineering materials for battery technology, setting a new benchmark for the development of safe, efficient, and long-lasting sodium-ion batteries.

5. Author Contributions

Roya Damircheli: Conceptualization, designing the methodology, conducting the experiments, analyzing the data, Writing – original draft.

Binh Hoang: Data analysis, Writing – review & editing.

Victoria Castagna Ferrari: Conducting the XPS experiment and analysis, Writing – review & editing.

Chuan-Fu Lin: Supervision, conceptualization, designing the methodology, conducting the experiments, analyzing the data, Writing – original draft.

6. Acknowledgment

This work was supported the U.S. Department of Energy, Office of Science, Office of Basic Energy Sciences, under Award Number DE-SC0024274. The authors would like to thank Dr. Jiancun Rao, from UMD Nanocenter Aimlab, for helping with the Hitachi SU-70 FEG SEM operational support.

7. References

1. Yabuuchi, N., Kubota, K., Dahbi, M. & Komaba, S. Research development on sodium-ion batteries. *Chemical Reviews* vol. 114 11636–11682 Preprint at https://doi.org/10.1021/cr500192f (2014).
2. Skundin, A. M., Kulova, T. L. & Yaroslavtsev, A. B. Sodium-Ion Batteries (a Review). *Russian Journal of Electrochemistry* vol. 54 113–152 Preprint at https://doi.org/10.1134/S1023193518020076 (2018).
3. Song, J., Xiao, B., Lin, Y., Xu, K. & Li, X. Interphases in Sodium-Ion Batteries. *Advanced Energy Materials* vol. 8 Preprint at https://doi.org/10.1002/aenm.201703082 (2018).
4. Kundu, D., Talaie, E., Duffort, V. & Nazar, L. F. The emerging chemistry of sodium ion batteries for electrochemical energy storage. *Angewandte Chemie - International Edition* vol. 54 3432–3448 Preprint at https://doi.org/10.1002/anie.201410376 (2015).
5. Nayak, P. K., Yang, L., Brehm, W. & Adelhelm, P. Von Lithium- zu Natriumionenbatterien: Vorteile, Herausforderungen und Überraschendes. *Angewandte Chemie* **130**, 106–126 (2018).
6. He, H., Sun, D., Tang, Y., Wang, H. & Shao, M. Understanding and improving the initial Coulombic efficiency of high-capacity anode materials for practical sodium ion batteries. *Energy Storage Mater* **23**, 233–251 (2019).
7. Xiao, L. *et al.* Low-Defect and Low-Porosity Hard Carbon with High Coulombic Efficiency and High Capacity for Practical Sodium Ion Battery Anode. *Adv Energy Mater* **8**, (2018).

8. Fan, L. & Li, X. Recent advances in effective protection of sodium metal anode. *Nano Energy* **53**, 630–642 (2018).
9. Wang, H., Wang, C., Matios, E. & Li, W. Facile Stabilization of the Sodium Metal Anode with Additives: Unexpected Key Role of Sodium Polysulfide and Adverse Effect of Sodium Nitrate. *Angewandte Chemie* **130**, 7860–7863 (2018).
10. Sun, Y., Shi, P., Xiang, H., Liang, X. & Yu, Y. High-Safety Nonaqueous Electrolytes and Interphases for Sodium-Ion Batteries. *Small* **15**, (2019).
11. Kim, Y.-J. *et al.* Enhancing the Cycling Stability of Sodium Metal Electrodes by Building an Inorganic–Organic Composite Protective Layer. *ACS Appl Mater Interfaces* **9**, 6000–6006 (2017).
12. Zhou, Z. *et al.* Ultra-Lightweight 3D Carbon Current Collectors: Constructing All-Carbon Electrodes for Stable and High Energy Density Dual-Ion Batteries. *Adv Energy Mater* **8**, (2018).
13. Seh, Z. W., Sun, J., Sun, Y. & Cui, Y. A Highly Reversible Room-Temperature Sodium Metal Anode. *ACS Cent Sci* **1**, 449–455 (2015).
14. Zhao, Y. *et al.* Natural SEI-Inspired Dual-Protective Layers via Atomic/Molecular Layer Deposition for Long-Life Metallic Lithium Anode. *Matter* **1**, 1215–1231 (2019).
15. Sun, B. *et al.* Dendrite-Free Sodium-Metal Anodes for High-Energy Sodium-Metal Batteries. *Advanced Materials* **30**, (2018).
16. Lin, C. F., Qi, Y., Gregorczyk, K., Lee, S. B. & Rubloff, G. W. Nanoscale Protection Layers to Mitigate Degradation in High-Energy Electrochemical Energy Storage Systems. *Acc Chem Res* **51**, 97–106 (2018).
17. Damircheli, R., Hoang, B., Castagna Ferrari, V. & Lin, C.-F. Fluorinated Artificial Solid–Electrolyte–Interphase Layer for Long-Life Sodium Metal Batteries. *ACS Appl Mater Interfaces* **15**, 54915–54922 (2023).
18. Wang, X. *et al.* Addressing the Low Solubility of a Solid Electrolyte Interphase Stabilizer in an Electrolyte by Composite Battery Anode Design. *ACS Appl Mater Interfaces* **13**, 13354–13361 (2021).
19. Guo, J., Wen, Z., Wu, M., Jin, J. & Liu, Y. Vinylene carbonate–LiNO3: A hybrid additive in carbonic ester electrolytes for SEI modification on Li metal anode. *Electrochem commun* **51**, 59–63 (2015).
20. Jia, W. *et al.* Extremely Accessible Potassium Nitrate (KNO_3) as the Highly Efficient Electrolyte Additive in Lithium Battery. *ACS Appl Mater Interfaces* **8**, 15399–15405 (2016).
21. Cheng, H. *et al.* Amorphous silicon nitride induced high dielectric constant toward long-life solid lithium metal battery. *Energy Storage Mater* **53**, 305–314 (2022).
22. Wu, C. Y., Chang, C. C. & Duh, J. G. Silicon nitride coated silicon thin film on three dimensions current collector for lithium ion battery anode. *J Power Sources* **325**, 64–70 (2016).
23. Liu, W., Liu, P. & Mitlin, D. Review of Emerging Concepts in SEI Analysis and Artificial SEI Membranes for Lithium, Sodium, and Potassium Metal Battery Anodes. *Adv Energy Mater* **10**, (2020).
24. Li, X. *et al.* Review on comprehending and enhancing the initial Coulombic efficiency of anode materials in lithium-ion/sodium-ion batteries. *Nano Energy* **77**, 105143 (2020).

25. Wang, J., Eng, C., Chen-Wiegart, Y. C. K. & Wang, J. Probing three-dimensional sodiation-desodiation equilibrium in sodium-ion batteries by in situ hard X-ray nanotomography. *Nat Commun* **6**, (2015).
26. Shylendra, S. P., Lonsdale, W., Wajrak, M., Nur-e-alam, M. & Alameh, K. Titanium nitride thin film based low-redox-interference po-tentiometric pH sensing electrodes. *Sensors (Switzerland)* **21**, 1–16 (2021).
27. Singh, P., Shivaprasad, S. M., Lal, M. & Husain, M. Angle-dependent XPS analysis of silicon nitride film deposited on screen-printed crystalline silicon solar cell. *Solar Energy Materials and Solar Cells* **93**, 19–24 (2009).
28. Smirnova, T. P. *et al.* SiCN alloys obtained by remote plasma chemical vapour deposition from novel precursors. *Thin Solid Films* **429**, 144–151 (2003).
29. Liu, S. *et al.* Designing Zwitterionic Gel Polymer Electrolytes with Dual-Ion Solvation Regulation Enabling Stable Sodium Ion Capacitor. *Adv Energy Mater* (2023) doi:10.1002/aenm.202300068.
30. Wang, X. *et al.* Addressing the Low Solubility of a Solid Electrolyte Interphase Stabilizer in an Electrolyte by Composite Battery Anode Design. *ACS Appl Mater Interfaces* **13**, 13354–13361 (2021).
31. Shi, P., Wang, X., Cheng, X. & Jiang, Y. Progress on Designing Artificial Solid Electrolyte Interphases for Dendrite-Free Sodium Metal Anodes. *Batteries* vol. 9 Preprint at https://doi.org/10.3390/batteries9070345 (2023).

Data Availability Statement

The data supporting the findings of this study are comprehensively detailed within the main manuscript, which includes all critical figures, and experimental results such as high-resolution SEM images, XPS spectra, EDS mappings, Nyquist plots, and cyclic deposition/stripping performance data. Additional supporting data, including extended analyses, supplementary figures, and detailed experimental procedures, are available in the Supplementary Information accompanying this article. The Supplementary Information provides in-depth methodological details, including the step-by-step process for fabricating the artificial solid electrolyte interphase (SEI) layers using silicon nitride (Si_3N_4), high-resolution top-view SEM images of various Si_3N_4/Na samples, and extensive XPS spectrum analyses of critical elements involved in the study.

Due to confidentiality and intellectual property considerations, certain raw data, including proprietary synthesis protocols and specific experimental details, cannot be publicly disclosed. However, the processed data, which have been rigorously analyzed and are essential for reproducing the findings of this study, are available upon reasonable request. Interested researchers should contact the corresponding author, Dr. Chuan-fu Lin, to discuss data access and any necessary agreements to ensure appropriate use and protection of the information.